Excess carrier lifetime and ambipolar diffusion anisotropy in a *nipi*-doped $In_{0.2}Ga_{0.8}As/GaAs$ multiple-quantum-well structure

H. T. Lin and D. H. Rich[a)]
Photonic Materials and Devices Laboratory, Department of Materials Science and Engineering, University of Southern California, Los Angeles, California 90089-0241

A. Larsson
Chalmers University of Technology, Department of Optoelectronics and Electrical Measurements, S-412 96 Göteborg, Sweden

(Received 3 January 1996; accepted for publication 26 January 1996)

The effects of strain-induced structural defects in a *nipi*-doped $In_{0.2}Ga_{0.8}As/GaAs$ multiple-quantum well sample were studied with time-resolved electron-beam-induced absorption modulation, in which carrier recombination lifetimes and ambipolar diffusion constants are measured with high spatial, spectral, and temporal resolution. Based on a phenomenological model, carrier lifetimes in the limit of weak excitation at room temperature were determined. The lifetime is found to be reduced by a factor of $\sim 10^{13}$ compared to a theoretically calculated value, owing to the presence of strain-induced defects and alternate recombination channels. By using a two-dimensional diffusion model, the ambipolar diffusion coefficients D_a along high-symmetry [110], [1$\bar{1}$0], and [10$\bar{0}$] directions were determined and resulted in an anisotropic behavior such that $D_a^{[110]} > D_a^{[1\bar{1}0]} > D_a^{[100]}$. The anisotropy in diffusion is attributed to corresponding asymmetries in the misfit dislocation density. © *1996 American Institute of Physics.* [S0021-8979(96)09709-6]

I. INTRODUCTION

Periodically doped *nipi* multiple-quantum well (MQW) structures are attractive for a wide variety of electro-optic device applications, including spatial light modulators (SLMs),[1] owing to large nonlinear optical effects that can be achieved from the doping. A high responsivity in photo-optic modulation of the effective *nipi* band gap, MQW excitonic absorption, and refractive index can be achieved by a relatively weak optical pumping in *nipi*-doped MQWs.[1,2] This is due to the photogenerated spatially separated electron–hole (e–h) plasma, which exhibits a long recombination lifetime and a large in-plane ambipolar diffusion constant.[3] Also, the large control over the plasma density in *nipi*-based SLM structures enables a spatial and quasi-optical modulation of the transmission and reflection of micro/millimeter waves for applications in phased-array signal processing, telecommunication, and radiometry, as recently demonstrated.[4,5] The determination of fundamental MQW-*nipi*-parameters, such as the excess carrier lifetime τ, and the ambipolar diffusion coefficient D_a, is of paramount importance in developing device applications and enhancing the basic understanding of nonlinear electro-optic effects and their interplay with strain relaxation.

The $In_xGa_{1-x}As/GaAs$ MQW system, owing largely to the transparent nature of the GaAs substrate with respect to the MQW interband transition energies, is a leading candidate for SLM device applications. In the $In_xGa_{1-x}As/GaAs$ MQW system, misfit dislocations and an associated Cottrell atmosphere of point defects[6] will be generated after a certain critical thickness has been reached. As is common in all strained systems and related electronic device applications such as high-electron mobility transistors (HEMTs)[7] and heterojunction phototransistors (HPTs)[8–10] based on $In_xGa_{1-x}As/GaAs$ heterojunctions, the strain-induced structural defects have a deleterious influence on excess carrier lifetime and transport. We have previously demonstrated the feasibility of using a novel technique called electron-beam-induced absorption modulation (EBIA)[11–14] to examine the influence of strain-induced defects on the excess carrier lifetime τ and the ambipolar diffusion coefficient D_a. In addition, we showed, using a 1D diffusion experiment, that an anisotropy in diffusive transport exists and is correlated with the difference in density of strain-induced defects along the high-symmetry $\langle 110 \rangle$ directions.[13] In this article we further extend our EBIA approach, utilizing a combination of a new time-resolved EBIA and a 2D Haynes–Shockley-type diffusive transport experiment to directly measure the excess carrier lifetime τ and the anisotropy of the ambipolar diffusion coefficient D_a. The variations in ambipolar diffusive transport along high-symmetry [110], [1$\bar{1}$0], and [100] directions are determined. This can possibly provide important information in understanding the influence of structural defects on transport in numerous devices based on InGaAs/GaAs.

II. EXPERIMENT

The *nipi*-doped MQW structure has been described previously, and a schematic of the band edges is shown in Fig. 1.[11–13] Briefly, it was grown by molecular-beam epitaxy on a GaAs(001) substrate and consists of 44 $In_{0.2}Ga_{0.8}As$ QWs, each 65 Å thick, and separated by 780-Å-thick GaAs barriers. In the center of each GaAs barrier a p-type Be-doping plane with a sheet density of 9.0×10^{12} cm^{-2} was inserted. On both sides of the QWs, using 100-Å-thick spacer layers, n-type Si-doping planes with a sheet density of 3.0×10^{12} cm^{-2} were inserted. The δ-doping planes induce a linear

a)Author to whom correspondence should be addressed; Electronic mail: danrich@alnitak.usc.edu

 0021-8979/96/79(9)/7014/7/$10.00

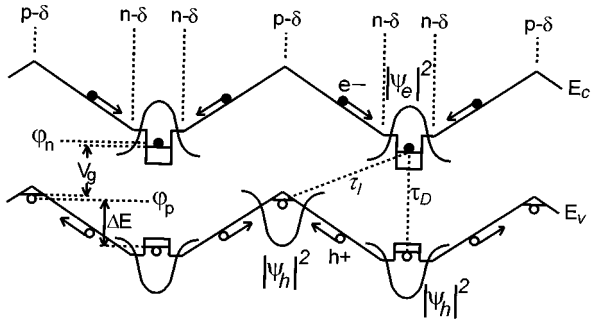

FIG. 1. Energy band diagram of the *nipi*-doped MQW structure. The structure is illustrated for the case of δ doping, which results in linear variations in the conduction (E_C) and valence (E_V) -band edges relative to the quasi-Fermi levels for electrons and holes (ϕ_n and ϕ_p, respectively).

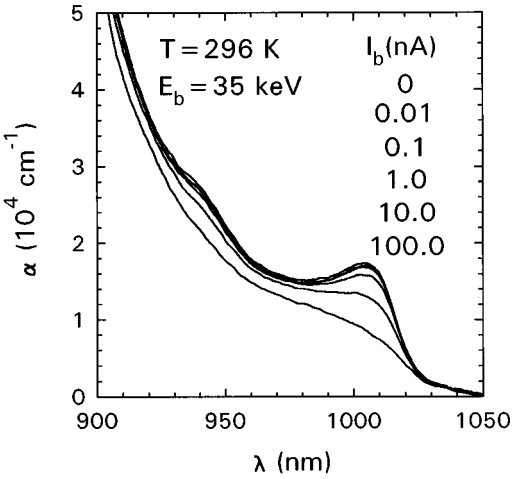

FIG. 3. EBIA spectroscopy measurement of the *nipi*-doped MQW sample at various probe currents I_b, at a temperature of $T=296$ K.

variation in the band edges along the growth direction and, during electron–hole pair generation, electrons will be attracted to the QWs and the holes to the barrier region midway between the wells, resulting in their spatial separation. In order to laterally confine the e–h plasma to a well-defined region, conventional lithographic techniques were used to pattern the sample into square mesas of $\sim 90\times 90\ \mu m^2$. An important aspect of *nipi*-doped semiconductors is that passivation of the side edges of a mesa is not required to prevent surface recombination of excess carriers since the majority carriers (excess electrons and holes in the n- and p-type regions, respectively) are essentially repelled from these edges. A nonpatterned planar region of $\sim 1\times 1\ cm^2$ was examined to study the effects of defects on the ambipolar diffusion of the e–h plasma.

In addition to employing the EBIA imaging and spectroscopy techniques as previously reported,[11–14] we have employed a new time-resolved EBIA approach which uses a boxcar integration technique, as illustrated in Fig. 2. In this approach, the wave form of the absorption modulation is reconstructed in order to determine the exponential decay of the trailing decay signal. A standard boxcar integration technique is used to sample the EBIA signal at various times after the electron beam is turned off in order to measure the decay time. The sampling frequency and e-beam blanking frequency is provided by a square wave reference signal with a frequency set to 100 Hz, giving a sampling interval of $t_{rep}=10$ ms. In the boxcar time scan mode, both the gate time (i.e., sampling window) t_s and the increment of time delay Δt_d are set to 100 μs, giving a total of 50 time channels along the decay curve. By integrating each gated signal over 300 sample-and-hole cycles, the scan readout time t_r, for each $\Delta\alpha$ versus time curve was ~ 150 s.

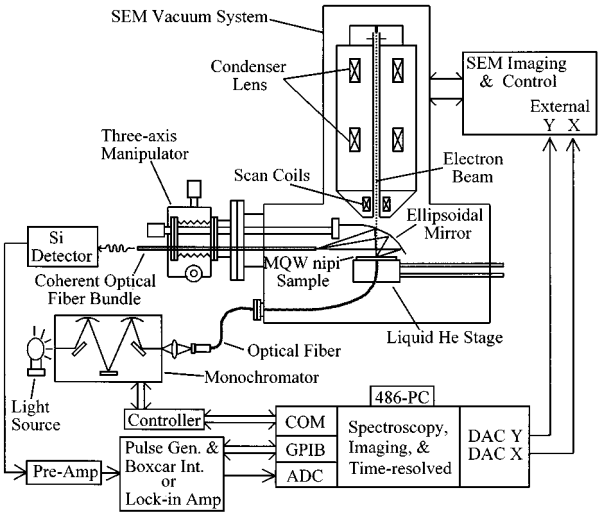

FIG. 2. Schematic of the time-resolved electron-beam-induced absorption-modulation (EBIA) setup.

III. RESULTS AND DISCUSSION

A. The excess carrier recombination time

Room-temperature EBIA spectra for various electron beam currents I_b are shown in Fig. 3. The effective QW absorption coefficients α were calculated according to $(-L_{\rm eff})^{-1}\ln T$, where T is the measured normalized transmission through the sample and $L_{\rm eff}$ is the total thickness of the QWs. The peak of the absorption spectrum at ~ 1005 nm is the $n=1$ heavy-hole to electron (hh1–e1) excitonic transition. During the continuous generation of e–h pairs by the high-energy (35 keV) electron beam, electrons and holes will be attracted to the QWs and the center of the barriers, respectively, resulting in their spatial separation, as illustrated in Fig. 1. Under sufficiently high excitation, the quenching of the hh1–e1 excitonic absorption occurs and is a result of band filling and screening of the Coulombic interaction of the excitons by the electron plasma filling of the QW states. A reliable treatment of screening in semiconductors requires the use of a many-body theory. For simplicity, however, the screening-induced change in α is often modeled by a simple absorption saturation relationship,[15,16]

$$\alpha=\frac{\alpha_0}{1+\delta n/n_{\rm sat}}+\alpha_b\,, \tag{1}$$

which is a heuristic fitting equation and not based on a theoretically derived model, where δn and n_{sat}, respectively, are the two-dimensional excess carrier density and the saturation carrier density, α_b is a band-to-band absorption term, and α_0 is the excitonic absorption coefficient in the absence of excitation. The experimental excitonic absorption α as an empirical function of δn will be determined from the following phenomenological model, and a deviation from the relationship of Eq. (1) will be discussed.

In the EBIA study here, e–h pairs can be generated nearly uniformly throughout the entire ~3.7 μm MQW region by a 35 keV electron beam.[17] The steady-state two-dimensional excess carrier density δn is given by[1,17]

$$\delta n = \frac{\tau P(1-\nu) I_b}{e E_i A_{\text{ex}}} \frac{dE_b}{dz}, \tag{2}$$

where τ is the lifetime, P is the *nipi* period, dE_b/dz is the electron beam ''depth-dose'' or energy dissipation function, I_b is the beam current, ν is the fractional beam loss due to backscattered electrons (for most cases, $\nu \ll 1$), e is the electric charge, E_i is the valence electron ionization energy, and A_{ex} is the effective lateral area of excitation. In Eq. (2), A_{ex} for the mesa is ~8100 μm^2, and the only unknown is τ, which can be described according to the phenomenological expression[1,14,18]

$$\tau = \tau_0 \exp\left(-\frac{e\beta\delta n}{2\epsilon}\right), \tag{3}$$

where τ_0 and β are parameters which depend on the temperature and the MQW *nipi* structure, and ϵ is the dielectric permittivity of GaAs. Insertion of Eq. (3) into Eq. (2) yields

$$\delta n = \frac{2\epsilon}{e} \theta I_b \exp\left(-\frac{e\beta\delta n}{2\epsilon}\right), \tag{4}$$

where

$$\theta = [\tau_0 P (dE_b/dz)(1-\nu)]/(2\epsilon A_{\text{ex}} E_i)$$
$$\approx 4278.8 \text{ kV/cm nA}.$$

Note that from the empirical electron energy loss model of Everhart and Hoff[17] we estimate that $dE_b/dz \approx 7.53$ keV/μm, and E_i is ~4.8 eV for GaAs. Since τ varies exponentially as a function of δn, the recombination rate, which is proportional to the reciprocal of lifetime τ, is no longer a constant when δn changes. The time-dependent δn in the absence of any carrier generation is given by

$$\frac{d}{dt}(\delta n) + \frac{\delta n}{\tau_0 \exp[-(e\beta\delta n)/(2\epsilon)]} = 0, \tag{5}$$

and integration, using a series expansion, yields

$$\ln(\delta n) + \sum_{n=1}^{\infty} \frac{1}{n} \frac{[-(e\beta\delta n)/(2\epsilon)]^n}{n!} = -\frac{t}{\tau_0} + \Delta,$$
$$\Delta = \ln(\delta n_0) + \sum_{n=1}^{\infty} \frac{1}{n} \frac{[-(e\beta\delta n_0)/(2\epsilon)]^n}{n!}, \tag{6}$$

where δn_0 is the initial steady state δn in the presence of I_b (i.e., before the electron beam is blanked), and can be determined numerically by Eq. (4), provided β and τ_0 are determined. In the limit of weak excitation, the differential excitonic absorption $\Delta\alpha$ to a first order of approximation is proportional to δn, according to Eq. (1). The experimental data of $\Delta\alpha$ vs t_d (the time delay after a steady-state excitation) at various I_b are shown in Fig. 4. The solid curves are the results of a nonlinear least-squares fit of these data at $I_b = 20$, 40, and 80 pA simultaneously to Eq. (6), yielding $\beta = 0.200\,74$ cm/kV and $\tau_0 = 3.08$ msec. Inserting the value of β and τ_0 into Eq. (4), therefore, allows for a determination of δn for various I_b. The experimental results of α vs δn and a fit to the model of Eq. (1) are shown in Fig. 5. The fit gives $n_{\text{sat}} = 2.5 \times 10^{11}$ cm^{-2}, consistent with previous estimates of n_{sat}.[15,19] The quenching of α is found to be more rapid than that described by Eq. (1) when $\delta n \gtrsim 1.5 \times 10^{11}$ cm^{-2}. The observed large deviation between the α vs δn curve and the fit of Eq. (1) in Fig. 5 is attributed to an absence of a treat-

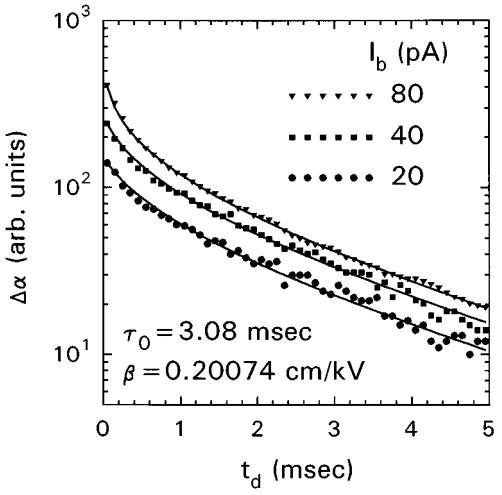

FIG. 4. Absorption modulation $\Delta\alpha$ as a function of time delay t_d (after a steady-state excitation) at various probe currents, $I_b = 20$, 40, and 80 pA. The solid curves are the results of a simultaneous nonlinear least square fit of Eq. (6) to the data.

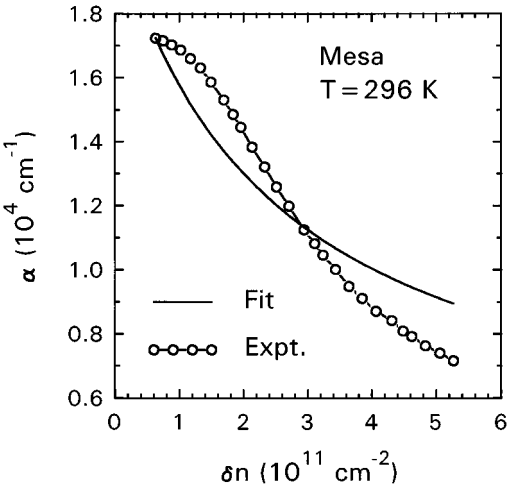

FIG. 5. Experimental and fitted α vs δn curves at $T = 296$ K.

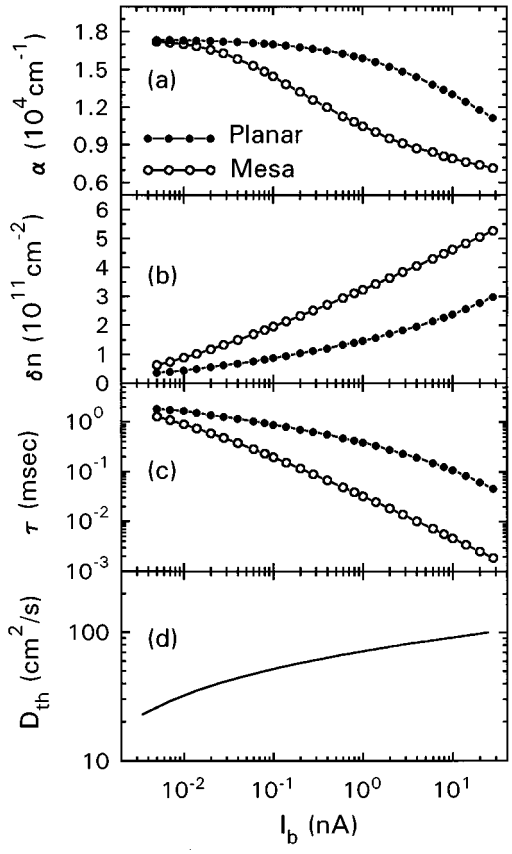

FIG. 6. Experimental results, using the phenomenological models of Eqs. (1)–(6), for (a) α, the absorption coefficient, (b) δn, the excess carrier density, (c) τ, the excess carrier lifetime, and (d) D_{th}, the theoretical ambipolar diffusion constant, as a function of I_b. Solid and open circles represent the data points for the planar and mesa regions, respectively.

ment of screening in the model of Eq. (1) which, as we show, should only be used as a rough approximation.

Further, using Eq. (3), the data of Fig. 5, and the values of β and τ_0, the relationships of δn and τ as a function of I_b in the planar and mesa regions can be determined and are shown in Fig. 6. The ambipolar diffusion length for this sample is $\sim$1 mm for $I_b=1$ nA.[13] The effect of the mesa walls is to confine the e–h plasma from diffusing beyond the 90 μm mesa widths, thereby leading to a larger δn in the mesa compared to the planar region for the same I_b. A theoretical calculation of the excess carrier lifetime τ_{th} by Jonsson *et al.*[19] yielded $\tau_{\text{th}} \approx 10^{10}$ s for an effective *nipi* barrier height of 1.257 eV for this *nipi* structure, which is $\sim$13 orders of magnitude greater than τ_0 determined here. The presence of structural defects which create additional recombination channels, not necessarily limited by the spatial separation, is evidently largely responsible for this reduction in lifetime.[10–13] Likewise, we have previously shown that, in another partially relaxed *nipi*-doped MQW structure under a weak excitation, a nearly 9 order of magnitude reduction of τ as compared to the theoretically calculated lifetime is attributed to the presence of defects which provide additional recombination channels.[14]

B. Anisotropy of the excess carrier diffusive transport

In EBIA imaging, we obtain images of the absorption modulation $\Delta\alpha$ as a function of the $x-y$ spatial position.[11] The MQW absorption coefficient for light that is transmitted at an energy corresponding to the first quantized heavy-hole to electron (hh1–e1) excitonic transition depends on the density of excess carriers situated near the center of the optical fiber. Since the presence of defects may impede the transport of carriers to the fiber center, a simple $x-y$ rastering of the e beam in the vicinity of the optical fiber will enable a mapping of the position of defects that impede the carrier transport. An EBIA grey-scale image, as shown in Fig. 7(a), was obtained by detecting the transmitted light at $\lambda=1005$ nm, corresponding to the hh1–e1 exciton absorption at the temperature of $T=296$ K. The electron beam, $I_b=1$ nA, was pulsed at a fixed frequency of $f=500$ Hz while rastered across the sample, and the signal was detected by a Si detector followed by a lock-in amplifier. An alternate view of this data is shown in Fig. 7(b), where the EBIA image is converted into a 3D plot [i.e., $\Delta\alpha$ vs (x,y) with the optical fiber center located at the origin] to show the behavior at small $\Delta\alpha$ far from the fiber center. The intensity steps in the image are a result of $\langle 110\rangle$-oriented defects which impede the transfer of excess electrons and holes to the fiber center. The position and orientation of these steps are further correlated with the position of dark line defects observed in cathodoluminescence (CL) imaging.[11–14]

In a 2D diffusive transport model, the time-dependent diffusion equation of excess carriers is given by

$$D_a \nabla^2 \delta n(\mathbf{r},t) - \frac{\delta n(\mathbf{r},t)}{\tau} + g_q(\mathbf{r},t) = \frac{\partial \delta n(\mathbf{r},t)}{\partial t}, \tag{7}$$

where $\delta n(\mathbf{r},t)$ is the spatially and temporally dependent excess carrier density, D_a is the ambipolar diffusion coefficient, and $\nabla^2 = \partial^2/\partial x^2 + \partial^2/\partial y^2$. The excess carrier generation rate, $g_q(\mathbf{r},t)$, can be approximated as

$$g_q(\mathbf{r},t) = \delta(\mathbf{r}-\mathbf{r}_0)[1+\sin(2\pi f t)],$$

where $\mathbf{r}_0$ is the position of the electron beam and f is the blanking frequency of the electron beam, and $\omega = 2\pi f$. The excitation can be regarded as a δ-function source since the electron-beam excitation volume ($\sim\mu$m) is much less than the diffusion length ($\sim$mm).[13] Equation (7) can be solved by using integration methods of Green's functions and Fourier transforms, and the steady-state solution is given by

$$\frac{\partial \delta n(r,t)}{\partial t} = A(\omega)\sqrt{\Psi^2+\Omega^2}\,\cos(\omega t), \tag{8}$$

where r is now the radial distance from the point of excitation $\mathbf{r}_0$, $A(\omega)$ is proportional to the intensity of excitation, and Ψ and Ω are the Fourier sine and cosine transforms of the Green's function $G(r,t)$, which is a solution to Eq. (7) when the source, $g_q(\mathbf{r},t)$, is set to $\delta(\mathbf{r}-\mathbf{r}_0)\delta(t)$. These functions are given by

$$\Psi = \int_0^\infty G(r,t)\cos(\omega t)\,dt$$

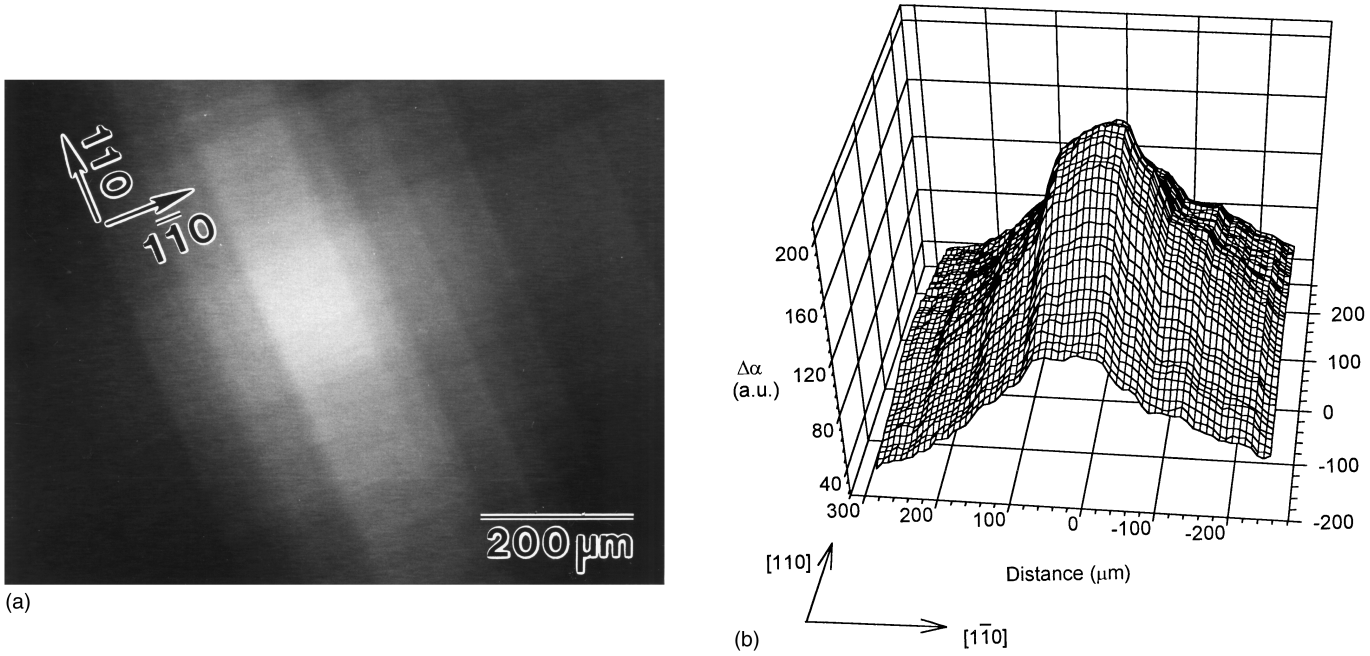

FIG. 7. EBIA image of the *nipi*-doped MQW sample at $\lambda=1005$ nm, corresponding to the e1–hh1 exciton absorption at $T=296$ K. A grey-scale representation showing the orthogonal nature of the steps is shown in (a) and 3D plot of this same image is shown in (b).

and

$$\Omega=\int_0^\infty G(r,t)\sin(\omega t)dt, \tag{9}$$

with the Green's function for the 2D diffusion equation,

$$G(r,t)=\frac{1}{t}\exp\left(-\frac{r^2}{4D_a t}\right)\exp\left(-\frac{t}{\tau}\right). \tag{10}$$

Ψ and Ω can further be expressed in terms of the modified Bessel functions of the second kind, $K_0(x)$, and

$$\Psi=i(2/\pi)^{1/2}[K_0(\eta)-K_0(\xi)]$$

and

$$\Omega=-(2/\pi)^{1/2}[K_0(\eta)+K_0(\xi)], \tag{11}$$

where $\eta=(r^2/D_a)^{1/2}(1/\tau+i\omega)^{1/2}$ and $\xi=(r^2/D_a)^{1/2}(1/\tau-i\omega)^{1/2}$.

In the limit of weak excitation, the excess carrier density δn is linearly proportional to $\Delta\alpha$ according to Eq. (1), and the excess carrier lifetime τ, as determined in Sec. III A, is 3.08 ms. The ambipolar diffusion coefficient D_a can therefore be determined by fitting Eq. (8) to an arbitrary line scan (intensity versus distance profile for a fixed ω) in the EBIA image of Fig. 7 with $r=0$ at optical fiber center. The results are shown in Fig. 8 for line scans and corresponding fits along the [110], [1$\bar{1}$0], and [100] directions. As expected, $\Delta\alpha$ decreases essentially in a fashion described by Eq. (8) for $r\gtrsim 75$ μm, with the exception of a steplike behavior, as indicated by the arrows. The steps, as seen in Fig. 7, are due to the defect-induced potential barriers which impede the diffusion of carriers and lead to a reduction in the effective D_a. Since the model does not attempt to account for discrete changes in diffusion, the fitting procedure only leads to an average diffusion constant. The flattening of the $\Delta\alpha$ vs r line profile for $r\lesssim 75$ μm is due to the finite size of the optical fiber (100 μm core diameter) which causes a deviation from the simple point source generation and detection model described by Eqs. (7)–(11). The best fit for each line profile gives an ambipolar diffusion coefficient D_a, as indicated in Table I.

The theoretical ambipolar diffusion coefficient $D_{\rm th}$ in a *nipi* structure with a uniform homogeneous excitation, as de-

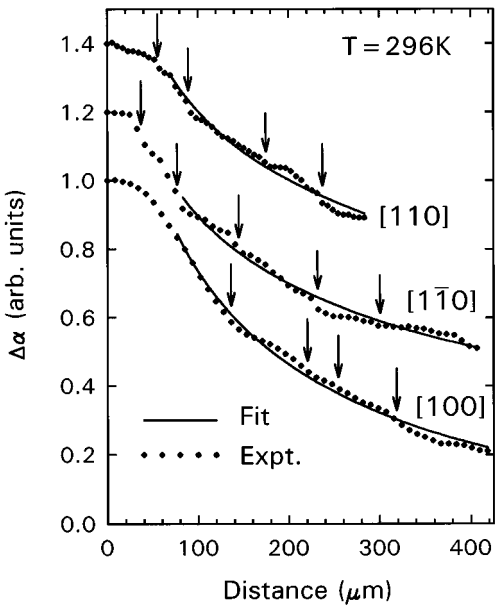

FIG. 8. Line scans of the absorption modulation vs distance from the optical fiber along high-symmetry [110], [1$\bar{1}$0], and [100]. The solid lines represent the best fit to the model of Eq. (8).

TABLE I. Ambipolar diffusion coefficient D_a, along high-symmetry [110], [1$\bar{1}$0], and [100] directions.

	[110]	[1$\bar{1}$0]	[100]
D_a (cm^2/s)	28.9±10.2	10.7±5.3	3.7±1.1

rived by Gulden *et al.*,[3] is dependent on the total excess carrier density as

$$D_{\text{th}}=\frac{1}{e^2}\frac{\sigma_n\sigma_p}{\sigma_n+\sigma_p}\frac{\partial\phi_{np}}{\partial n}, \tag{12}$$

where $\sigma_n=ne\mu_n$ and $\sigma_p=pe\mu_p$ are the n- and p-layer conductivities, n and p are the average 3D excess carrier densities which are given by $\delta n_e/P$ and $\delta n_h/P$, respectively, and $\phi_{np}=\phi_n-\phi_p$ is the difference in quasi-Fermi levels. The 2D excess hole density, δn_h, is given by $\delta n_h\approx\delta n_e+\delta N_A$, since most of the dopants are ionized at room temperature. An excess p doping of $\delta N_A=3.0\times10^{12}$ cm^{-2} as compared to n-doping was inserted in order to locate the Fermi level sufficiently far below the electron ground state in the QWs to ensure that the QWs are essentially free from electrons under thermal equilibrium. The lower limit for the ideal mobilities μ_n and μ_p are estimated to be ~3100 and ~170 cm^2/V s, respectively, for equivalent 3D doping densities in GaAs.[20] For the present δ-doped *nipi* structure, $\partial\phi_{np}/\partial n$ is approximately a constant[3] and is given by $\partial\phi_{np}/\partial n=(eP)^2/4\epsilon$. The theoretical diffusion coefficient D_{th} versus I_b, taking into account the excess p doping, is plotted in Fig. 6(d). An increase of ~20% in D_{th} as I_b increases from 0.1 to 1 nA is observed. This indicates that the excitation dependence of D_a is small for $I_b\lesssim1$ nA, i.e., in the limit of weak excitation. As a result, D_a is expected to approach a constant as δn vanishes, further justifying the constant value for D_a used in the model of Eqs. (7)–(11). We note that the actual limit of D_{th} as I_b vanishes for this structure is uncertain as a result of the large uncertainty in δn_e and the Fermi-level position relative to the e1 ground state under thermal equilibrium when there is no excitation.

We have demonstrated previously that the orientation and positions of steps (as indicated by the arrows in Fig. 8) seen in the absorption modulation strongly correspond with the orientation and positions of dark line defects (DLDs) seen in the CL image.[11,12] This has been attributed to the presence of structural defects such as dislocations and point defects that

(i) change the band gap due to a local reduction in strain, thereby creating a barrier to diffusive transport, and
(ii) create fast nonradiative recombination centers, which reduce δn as the plasma traverses the DLD region.[12–15]

For strained III–V heterostructures, an asymmetry in the density of orthogonal ⟨110⟩ 60° dislocations has been attributed to the substrate miscut,[21,22] the different levels of stress required to generate the α and β misfit dislocation cores, and differences in α and β dislocation glide velocities.[23,24] Further, due to the chemical inequivalence of the α and β dislocation cores, it is plausible each of the dislocation types will impact differently the extent to which the e–h plasma transport is impeded and nonradiative recombination occurs, aside from differences in the dislocation density. The asymmetry in D_a summarized in Table I is consistent with that obtained in a 1D diffusion experiment.[13] That experiment involved patterning the sample into 90 μm stripes along the orthogonal ⟨110⟩ directions and determining the linear DLD density along both the directions. As argued in Ref. 13, an enhanced density of DLDs along [1$\bar{1}$0] leads to a corresponding reduction in D_a along [110], consistent with the present results of our 2D diffusion experiment, as seen in Table I. For diffusion along [100], however, the carriers must traverse both [110] and [1$\bar{1}$0] DLD regions. This accounts for the noticeable reduction of D_a along [100] since the local DLD density along [100], i.e., $\rho_{[100]}$, can be related to $\rho_{[110]}$ and $\rho_{[1\bar{1}0]}$ by

$$\rho_{[100]}=\frac{1}{\sqrt{2}}(\rho_{[110]}+\rho_{[1\bar{1}0]}). \tag{13}$$

Thus, it is our observation that when $\rho_{[110]}\simeq\rho_{[1\bar{1}0]}$, an increase in average defect density along [100] may be responsible for the reduction of D_a relative to D_a along the $\rho_{[110]}$ and $\rho_{[1\bar{1}0]}$ directions. Also, as previously observed,[13] the scaling of D_a with the linear density of DLDs is not necessarily linear since the thermal activation energy for diffusion is also different along both directions. Large standard deviations of D_a are also obtained from the fitting, as listed in Table I. This may be attributed to local variations in the DLD density along the scan line, and acts to induce further deviation from our simple 2D diffusion model.

IV. CONCLUSION

In conclusion, we have quantitatively examined the deleterious influence of structural defects on excess carrier lifetime and diffusive transport with the use of a new time-resolved EBIA technique. A factor of ~10^{13} in the reduction of lifetime in the limit of weak excitation compared to theoretical estimates was found. The ambipolar diffusion constants were measured using an optical 2D Haynes–Shockley-type experiment, where solutions to the 2D time-dependent diffusion equation were used to obtain the direction dependence of D_a, in the limit of weak excitation. An anisotropy was measured and attributed to differences in defect densities along the orthogonal ⟨110⟩ directions. In addition to the anisotropy of D_a along [110] and [1$\bar{1}$0], D_a along [110] is found to be lowest and is attributed to a superposition and an orientational dependence of the [110] and [1$\bar{1}$0] defects.

ACKNOWLEDGMENTS

This work was supported by the U.S. Army Research Office and National Science Foundation (RIA-ECS).

[1] J. Maserjian, P. O. Andersson, B. R. Hancock, J. M. Iannelli, S. T. Eng, F. J. Grunthaner, K.-K. Law, P. O. Holtz, R. J. Simes, L. A. Coldren, A. C. Gossard, and J. L. Merz, Appl. Opt. **28**, 4801 (1989).
[2] G. H. Döhler, IEEE J. Quantum Electron. **QE-22**, 1682 (1986); J. Vac. Sci. Technol. B **1**, 278 (1983).
[3] K. H. Gulden, H. Lin, P. Kiesel, P. Riel, G. H. Döhler, and K. J. Ebeling, Phys. Rev. Lett. **66**, 373 (1991).

[4] M. K. Hibbs-Brenner, P. P. Ruden, J. A. Lehman, J. J. Liu, and R. A. Walterson, IEEE J. Quantum Electron. **QE-30**, 1227 (1994).
[5] G. Delgado, J. Johansson, A. Larsson, and T. Andersson, IEEE Microwave Guided Wave Lett. **MGW-5**, 198 (1995).
[6] D. H. Rich, K. C. Rajkumar, L. Chen, A. Madhukar, T. George, J. Maserjian, F. J. Grunthaner, and A. Larsson, J. Vac. Sci. Technol. B **10**, 1965 (1992).
[7] M. Meshkinpour, M. S. Goorsky, and K. M. Matney, J. Appl. Phys. **76**, 3362 (1994).
[8] O. Sjölund and A. Larsson, IEEE Photonics Technol. Lett. **PTL-7**, 682 (1995).
[9] O. Sjölund, M. Ghisoni, and A. Larsson, Electron. Lett. **31**, 917 (1995).
[10] H. T. Lin, D. H. Rich, O. Sjölund, M. Ghisoni, and A. Larsson, J. Appl. Phys. (in press).
[11] D. H. Rich, K. Rammohan, Y. Tang, H. T. Lin, J. Maserjian, F. J. Grunthaner, A. Larsson, and S. I. Borenstain, Appl. Phys. Lett. **63**, 394 (1993).
[12] D. H. Rich, K. Rammohan, Y. Tang, H. T. Lin, J. Maserjian, F. J. Grunthaner, A. Larsson, and S. I. Borenstain, J. Vac. Sci. Technol. B **11**, 1717 (1993).
[13] D. H. Rich, K. Rammohan, Y. Tang, H. T. Lin, J. Maserjian, F. J. Grunthaner, A. Larsson, and S. I. Borenstain, Appl. Phys. Lett. **64**, 730 (1994).
[14] D. H. Rich, H. T. Lin, and A. Larsson, J. Appl. Phys. **77**, 6557 (1995).
[15] S. H. Park, J. F. Morhange, A. D. Jeffery, R. A. Morgan, A. Chavez-Pirson, H. M. Gibbs, S. W. Koch, N. Peyghambarian, M. Derstine, A. C. Gossard, J. H. English, and W. Weigmann, Appl. Phys. Lett. **52**, 1201 (1988).
[16] M. Kawase, E. Garmire, H. C. Lee, and P. D. Dapkus, IEEE J. Quantum Electron. **QE-30**, 981 (1994).
[17] T. E. Everhart and P. H. Hoff, J. Appl. Phys. **42**, 5837 (1971).
[18] J. M. Iannelli, J. Maserjian, B. R. Hancock, P. O. Andersson, and F. J. Grunthaner, Appl. Phys. Lett. **54**, 301 (1989).
[19] B. Jonsson, A. G. Larsson, O. Sjölund, S. Wang, T. G. Andersson, and J. Maserjian, IEEE J. Quantum Electron. **QE-30**, 63 (1994).
[20] S. M. Sze, *Physics of Semiconductor Devices*, 2nd ed. (Wiley, New York, 1981), p. 29.
[21] D. H. Rich, K. Rammohan, Y. Tang, H. T. Lin, R. S. Goldman, H. H. Wieder, and K. L. Kavanagh, J. Vac. Sci. Technol. B **13**, 1766 (1995).
[22] K. Rammohan, Y. Tang, D. H. Rich, R. S. Goldman, H. H. Wieder, and K. L. Kavanagh, Phys. Rev. B **51**, 5033 (1995).
[23] T. George, E. R. Weber, S. Nozaki, T. Yamada, M. Konagai, and K. Takahashi, Appl. Phys. Lett. **59**, 60 (1991).
[24] E. A. Fitzgerald, G. P. Watson, R. E. Proano, D. G. Ast, P. D. Kirchner, G. D. Pettit, and J. M. Woodall, J. Appl. Phys. **65**, 2220 (1989).